ELSEVIER

Microelectronics Journal 38 (2007) 151–156

Microelectronics Journal

www.elsevier.com/locate/mejo

Electrical characterization of analogue and RF integrated circuits by thermal measurements

D. Mateo*, J. Altet, E. Aldrete-Vidrio

Electronic Engineering Department, Universitat Politècnica de Catalunya, C/. Jordi Girona 1–3, Campus Nord UPC, Edifici C4, 08034 Barcelona, Spain

Received 28 December 2005; received in revised form 31 July 2006; accepted 17 August 2006
Available online 16 October 2006

Abstract

This paper presents a novel technique for measuring the electrical characteristics of analogue circuits, based on measuring the temperature at the silicon surface close to the circuit under test. As a detailed example, the paper analyses how the gain of an amplifier can be observed through temperature measurements. Experimental results validate the feasibility of the technique. Simulated results show how this technique can be used to measure the bandwidth and central frequency of a 2.4 GHz low noise amplifier (LNA) designed in a 0.35 μm standard CMOS technology.
© 2006 Elsevier Ltd. All rights reserved.

Keywords: Analogue integrated circuits; RF testing; Analogue testing; Thermal testing; Temperature measurements

1. Introduction

The scaling down of CMOS technologies has enabled a whole system to be integrated on a single silicon chip (System on Chip, SoC). The benefits of this are low cost, high reliability and low power consumption. A drawback of SoC integration is the significant loss of observability that it entails, since few nodes are accessible from the outside. As a consequence, the complexity and cost of testing, monitoring and characterizing individual parts of the system increase, specifically in RF front-ends in which the operating frequency is in the range of gigahertz [1].

The characterization and testing of RF integrated circuits (RFIC) SoC is carried out at system level by measuring high level performances such as bit error rate (BER) and error vector magnitude (EVM) [2]. However, during the debugging phase of a product, the possibility of characterizing the different blocks individually (Low Noise Amplifier, Mixer, Local Oscillator, etc.) is of great help. Different solutions have been proposed for increasing the observability of internal nodes in RFICs, in order to perform electrical measurements [3–8]. Requirements for these strategies are: there must be an inappreciable loading effect on the circuit under test (CUT) and, when the tester is built together with the CUT, the area overhead must be as low as possible.

This paper presents a novel procedure for characterizing high frequency and RF analogue circuits. This consists of measuring the temperature at the silicon surface, close to the circuit under test (CUT). As we will see in this paper, the amplitude of some spectral components of the temperature near the CUT depends on the electrical characteristics of the circuit.

Measuring temperature to determine electrical characteristics is an innovative and attractive solution, as the CUT is not electrically loaded. The temperature measuring system gets the information from the intrinsic thermal coupling provided by the silicon substrate. Thus, the electrical performance of the CUT is unaffected. Temperature can be sensed with embedded sensors, which would allow in-field testing, or with external temperature sensors [9].

This paper is organized as follows: Section 2 explains the principle of the procedure. Section 3 includes experimental measurements that validate the procedure's feasibility. Section 4 shows an application of the technique, based

*Corresponding author. Tel.: +34 93 4016748; fax: +34 93 401 6756.
E-mail address: mateo@eel.upc.edu (D. Mateo).

0026-2692/$ - see front matter © 2006 Elsevier Ltd. All rights reserved.
doi:10.1016/j.mejo.2006.08.003

on simulated results: the bandwidth and central frequency of a 2.4 GHz LNA designed using a 0.35 μm CMOS technology are estimated. Finally, some conclusions are presented in Section 5.

2. The principle of the technique

The proposed technique is based on four properties of the electrical circuits implemented in ICs:

(i) The relation between the power dissipated by a device/circuit and its electrical characteristics.
(ii) The frequency shift that can be observed in the spectral components of the power dissipated by a device/circuit when compared with the spectral components of the electrical signals that drive it.
(iii) The thermal coupling provided by the silicon die, which allows dissipated power to be observed by measuring the temperature.
(iv) The transfer function of the thermal coupling: it behaves as a low pass filter and only allows the thermal observation of the low frequency spectral components of the power dissipated by a device or circuit.

To illustrate the first two properties, let us consider a linear resistor R. When driven with a voltage sum of two tones of amplitude A and frequencies f_1 and f_2

$$V_{\text{in}}(t) = A(\cos(2\pi f_1 t) + \cos(2\pi f_2 t)) \tag{1}$$

its dissipated power is

$$P(t) = \frac{A^2}{2R}(2 + 2\cos(2\pi(f_2 - f_1)t) + 2\cos(2\pi(f_2 + f_1)t) + \cos(2\pi 2 f_2 t) + \cos(2\pi 2 f_1 t)). \tag{2}$$

As it can be seen, the electrical signals only have spectral content at frequencies f_1 and f_2, whereas the power dissipated has spectral components at f_2–f_1, f_1+f_2, $2f_1$ and $2f_2$. This effect can be called frequency mixing. In the case of a resistor driven with (1) plus a DC bias, other spectral components of power appear, for instance, at f_1 and f_2. In addition, the amplitudes of the spectral components of the dissipated power depend on the value of R, i.e. they carry information about the electrical characteristics of the circuit considered.

To present how these concepts can be applied to observing the gain of an amplifier, let us consider the common source amplifier in Fig. 1. In general, the current through the MOS transistor, $I_s(t)$, can be written as

$$I_S(t) = I_{DC} + f(V_{\text{in}}(t)), \tag{3}$$

where $V_{\text{in}}(t)$ is the signal applied to the amplifier's input, I_{DC} is the bias current generated by the DC bias applied to the MOS gate (not drawn in the figure) and $f(V_{\text{in}}(t))$ is the transconductance function of the MOS.

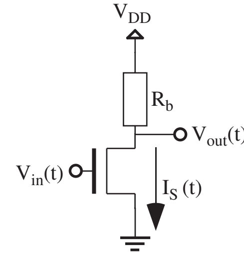

Fig. 1. Simple common source amplifier.

The simplest (and ideal) transconductance function for an amplifier is the linear relationship

$$f(V_{\text{in}}(t)) = K_1 V_{\text{in}}(t), \tag{4}$$

where K_1 is the linear transconductance factor of the MOS transistor. If the input voltage is the sum of two tones of amplitude A and frequencies f_1 and f_2, the analysis of the circuit shows that the power dissipated has many spectral components, as in the resistor case. Specifically, the amplitude of the spectral component dissipated by the MOS transistor at frequency f_2–f_1 is

$$P_{f_2-f_1} = -R_b K_1^2 A^2 = -\frac{A_v^2}{R_b} A^2, \tag{5}$$

where A_v is the amplifier's linear voltage gain defined as $R_b K_1$, and R_b is the load resistance. According to the above expression, the magnitude of such a spectral component depends on the gain of the amplifier A_v, the load resistor R_b and the amplitude A. Note that the sign of (5) only means a phase delay of 180° with respect to the input signal.

If we have a frequency dependent transconductance $K_1(f)$, expression (5) becomes

$$P_{f_2-f_1} = -R_b K_1(f_1) K_1(f_2) A^2 = -\frac{A_v(f_1) A_v(f_2)}{R_b} A^2. \tag{6}$$

The spectral component of the dissipated power at frequency f_2–f_1 has many interesting properties:

(i) In (5) its amplitude is independent of the absolute value of the frequencies f_1 and f_2, and it is strongly dependent on the electrical characteristics of the circuit, in this case, the voltage gain. This is true as long as the gain of the amplifier is frequency independent.
(ii) From (6) it is clear that the amplitude of the power dissipated at f_2–f_1 depends on the characteristics of the circuit at the high frequencies f_1 and f_2: in this example the gain at these frequencies.
(iii) The location of this component in the spectrum of the power dissipated depends only on the difference between such frequencies. It is independent from the absolute values of f_2 and f_1.
(iv) If the electrical signals at f_1 and f_2 are in the order of hundreds of MHz to a few GHz (the usual values in RF wireless communication systems), it is impossible to measure the temperature corresponding to the heat

flow produced at such high frequencies, as thermal coupling in the silicon substrate behaves as a low pass filter [9,10]. However, if f_2-f_1 is small enough, it will be possible to estimate the power dissipated at this low frequency by measuring the same spectral component of the temperature near the CUT.

Therefore, the technique proposed in this paper consists in driving a circuit with the sum of two tones. If the spectral component of the power dissipated at f_2-f_1 carries information about the electrical characteristics of the circuit at high frequencies, these characteristics can be derived by thermal measurements at f_2-f_1.

Now, if we consider again the case of the common source amplifier in Fig. 1, but take into account nonlinearities up to the third-order in the transconductance function, then:

$$f(V_{\mathrm{in}}(t)) = K_1V_{\mathrm{in}}(t) + K_2V_{\mathrm{in}}^2(t) + K_3V_{\mathrm{in}}^3(t), \tag{7}$$

where K_2 and K_3 are the second- and third-order transconductance factors of the MOS transistor, respectively. The power dissipated by the transistor at f_2-f_1 is

$$\begin{aligned} P_{f_2-f_1} = {} & (-R_{\mathrm{b}}K_1^2A^2) \\ & + (V_{\mathrm{DD}}K_2A^2 - 3R_{\mathrm{b}}K_2^2A^4 - 2R_{\mathrm{b}}I_{\mathrm{DC}}K_2A^2) \\ & + \left(-6R_{\mathrm{b}}I_{\mathrm{DC}}K_1K_3A^4 - \tfrac{75}{8}R_{\mathrm{b}}K_3^2A^6\right). \end{aligned} \tag{8}$$

Comparing this expression with (5), we can observe that there is a significant increase in its complexity, although it still carries information about the circuit's electrical characteristics. The first term in parentheses corresponds to the linear behaviour of the amplifier (see (5)). The nonlinearity of second-order is responsible for the second term in parentheses, while the last term is due to the third-order's nonlinearity. In a well-designed, highly linear amplifier, the gain should be much higher than the nonlinearities. In such a case, together with the use of a small amplitude A for the input signal, the first term in parentheses will dominate over the others. Therefore, it would be possible to obtain information about the gain by estimating the dissipated power.

Finally, the accurate generation of two tones at high frequency with such close frequencies is directly possible with commercial vector signal generators (e.g. [11]). The value of (f_2-f_1) has to be lower than the cut-off frequency of the thermal coupling mechanism in the silicon substrate. In addition, the thermal coupling attenuates as the distance between the dissipating device/circuit and the temperature sensor increases. This attenuation is frequency dependent; it is higher for the higher frequency components of the dissipated power. Examples are illustrated in [9,12,13]. A consequence of this physical effect is that a temperature sensor can record the power dissipated by devices placed inside a circle of radius R. The centre of this circle is the temperature sensor's location, and the value of R is frequency dependent (the lower the frequency, the larger the value of R). Therefore, there is a trade-off in choosing the value of (f_2-f_1): on the one hand, low values of (f_2-f_1) would allow greater distances between the dissipating device and the temperature sensor. On the other hand, low values of (f_2-f_1) may imply that a temperature sensor is potentially able to observe the power dissipated by many devices, which may mask the measurement of the power dissipated by the device of interest.

3. Feasibility of the technique

The goal of this section is to show the feasibility of the temperature measurements needed to track the spectral content of the power dissipated at f_2-f_1. The aim is also to experimentally validate the theoretical analysis of the spectral components of the power dissipated by a device, in this case, a MOS transistor in diode configuration (Fig. 2).

Fig. 3 shows the layout of the IC used in the experiment. It contains MOS devices in diode configuration (Fig. 2), which behave as dissipating devices, and a differential temperature sensor embedded in the same silicon die. The output voltage of differential temperature sensors is proportional to the difference of temperature at two points on the silicon surface. In our case, the temperatures at the sensing points are named $T_1(t)$ and $T_2(t)$ [9,12].

The aspect ratio of the dissipating device is $\frac{10}{1.2}$. It is placed at 47 μm from the temperature monitoring point

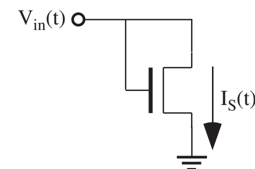

Fig. 2. NMOS in diode configuration.

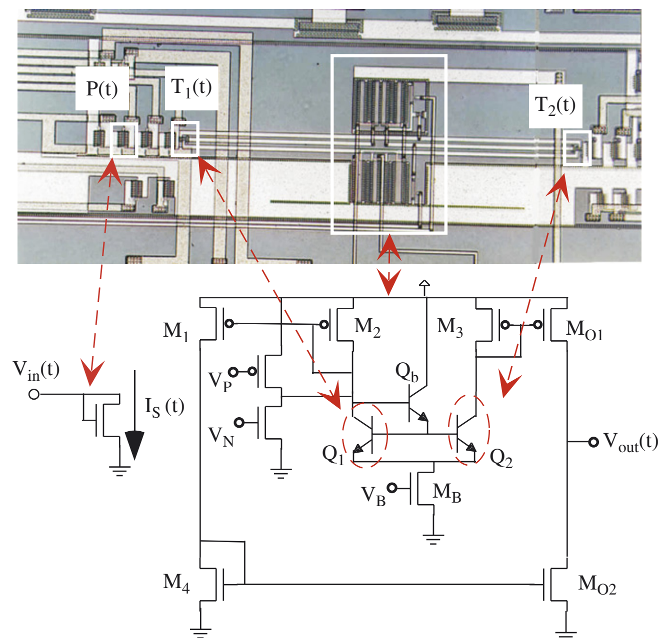

Fig. 3. Experimental set-up and sensor schematic.

$T_1(t)$. Using Sah's model for the transistor and taking into account the degeneration of the mobility due to short channel effects, the expression of the current through the device is expressed by [14]

$$I_S(t) = \frac{K(V_{in}(t) - V_t)^2}{2(1 + \theta(V_{in}(t) - V_t))}, \qquad (9)$$

where $V_{in}(t)$ is the gate to source voltage, V_t is the threshold voltage, K is the transconductance of the MOS transistor and θ models the degeneration of the mobility due to short channel effects. By expanding it into a Taylor series and taking into account up to the cubic term (the consideration of the mobility degeneration makes the third-order term appear), it is possible to obtain a polynomial expression for the current, which is valid for $V_{in}(t) > V_t$, and more easily manageable for our purposes

$$I_S(t) \approx m_0 + m_1 V_{in}(t) + m_2 V_{in}^2(t) + m_3 V_{in}^3(t). \qquad (10)$$

Fig. 4 shows the I/V DC characteristic of the dissipating device. The values of the m's coefficients in (10) that fit the measurements are:

$$m_0 = -0.14 \times 10^{-3}, \quad m_1 = -0.25 \times 10^{-3}, \quad m_2 = 0.56 \times 10^{-3}, \quad m_3 = -49.74 \times 10^{-6}. \qquad (11)$$

If we also apply two tones of amplitude A at the input, plus a V_{DC} term for polarizing the diode

$$V_{in}(t) = V_{DC} + A(\cos(2\pi f_1 t) + \cos(2\pi f_2 t)) \qquad (12)$$

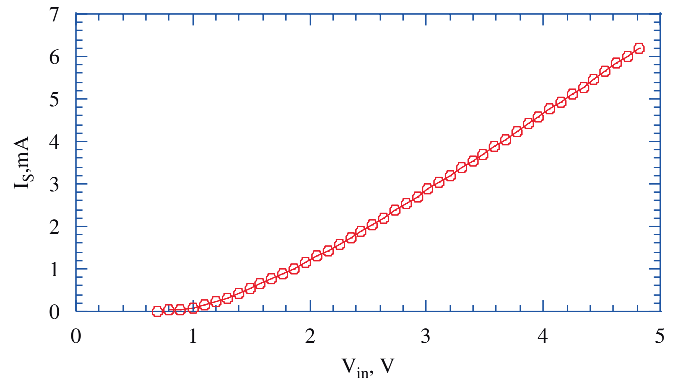

Fig. 4. I/V DC characteristic of the dissipating MOS transistor.

the amplitude of the power dissipated by the MOS transistor at frequency (f_2–f_1) is

$$P_{f_2-f_1} = (A^2 m_1 + 3A^2 m_2 V_{DC} + 6A^2 m_3 V_{DC}^2 + 3A^4 m_3). \qquad (13)$$

An analysis of this expression shows that the first term $A^2 m_1$ corresponds to the linear behaviour of the diode (similar to the case of the resistor and the amplifier). The other three terms correspond to the nonlinearity of the diode.

To observe this spectral component of the power by measuring temperature, Fig. 5 (left) shows the experimental set-up used. The dissipating device is activated by two sinusoidal voltage sources of frequencies f_1 and f_2, plus a DC voltage (as stated in Eq. (12)).

The sensor's output is connected to a spectrum analyser. Fig. 5 (right) shows the spectrum obtained when $f_1 = 1\,\text{kHz}$ and $f_2 = 1.130\,\text{kHz}$. In this figure, the sensor's output voltage components at f_2–f_1, $2f_1$–f_2, $2f_2$–f_1, f_1 and f_2 are clearly observed.

To validate expression (13), we have replaced the spectrum analyzer of Fig. 5 with a Lock-in Amplifier. Fig. 6 shows the amplitude of the spectral component at f_2–f_1 of the sensor's output voltage, $V_{OUT|f1-f2}$, versus amplitude A (see Eq. (12)). We have fixed f_2–f_1 at 1 kHz for

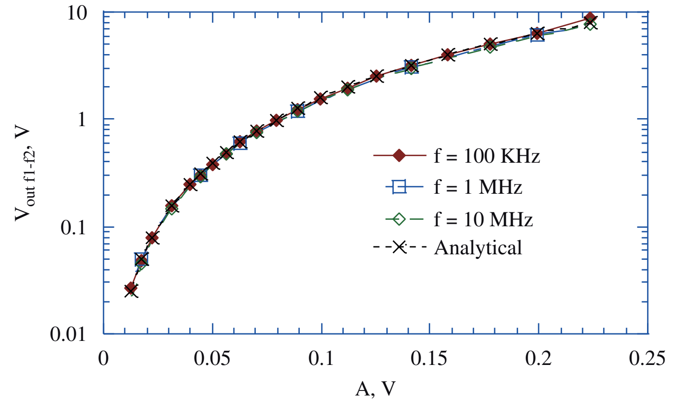

Fig. 6. Amplitude measurements from the look-in amplifier ($V_{OUT|f1-f2}$ sensor), and Eq. (13) multiplied by the sensitivity of the sensor (all values are at f_2–f_1)

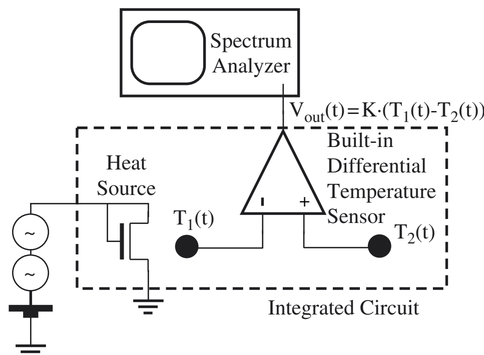

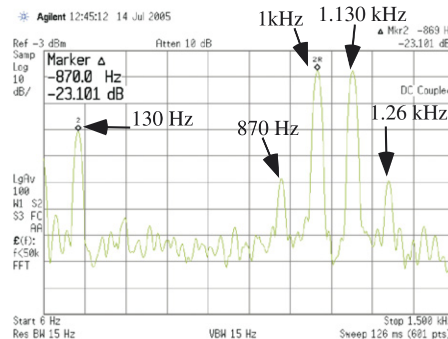

Fig. 5. Experimental set-up (left) and temperature sensor output spectrum (right).

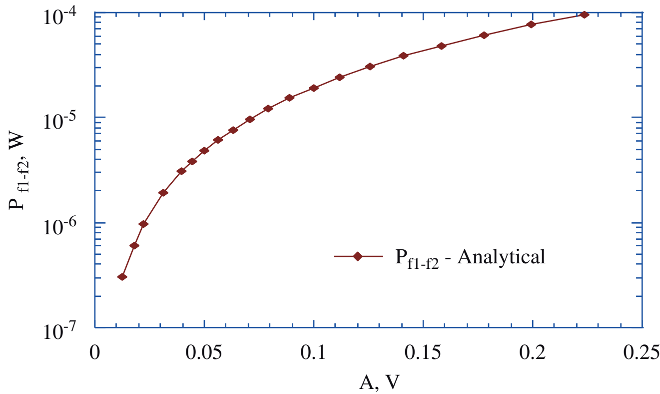

Fig. 7. Power amplitude estimation at (f_2–f_1) from analytical Eq. (13).

three different values of f_1: 100 kHz, 1 MHz and 10 MHz. V_{DC} was fixed to 2 V.

Additionally, the estimated amplitude of the sensor's output is plotted in the same figure. This was obtained by multiplying the analytical expression (13) by the DC sensitivity of the sensor (81 V/W [12]). Fig. 7 shows the power amplitude at (f_2–f_1) estimated from analytical Eq. (13).

From these two figures we observe:

(i) By comparing the amplitude of the Vout spectral component at (f_2–$f1$), $V_{OUT|f1-f2}$, for the three values of $f1$, we can see that such amplitudes do not depend on the absolute value of f_1. This means that m's coefficients in expression (13) do not depend on the frequency in the range considered.

(ii) We also observe a good match between the measured and the estimated output voltage $V_{OUT|f1-f2}$, which validates the analysis performed. The figure also demonstrates that the sensitivity of the sensor is constant in the band from DC to 1 kHz.

(iii) We can also observe from Fig. 7 that power dissipation magnitudes lower than 1 μW can be detected with temperature sensors embedded with the CUT.

4. Application of the technique

In this section we consider a tuned amplifier whose gain is frequency dependent. The amplitude of the power dissipated at f_2–f_1 depends on the gain of the amplifier. Therefore, if the values of f_1 and f_2 are swept (keeping the value f_2–f_1 constant), then it is possible to obtain the bandwidth and the central frequency of amplifiers by plotting the magnitude of the dissipated power at f_2–f_1 as a function of f_1.

The circuit considered is a fully differential 2.4 GHz Low Noise Amplifier (see Fig. 8) designed using a 0.35 μm CMOS technology. Its electrical performances are: 24 dB voltage gain (16 in linear), 15 dB input return loss, 5 dB NF, −10 dBm 1 dB compression point and 10 mA DC current consumption. We applied two tones of equal

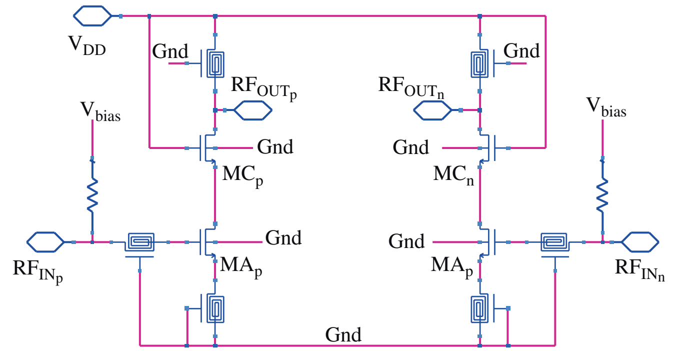

Fig. 8. LNA circuit schematic.

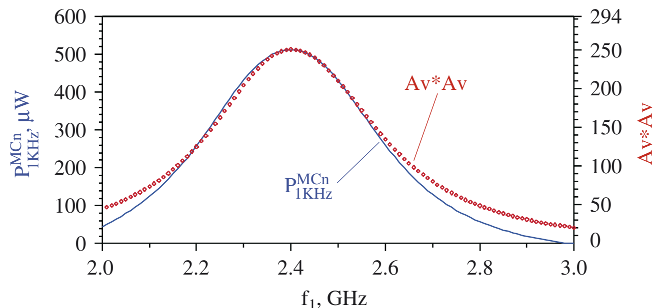

Fig. 9. LNA squared voltage gain (right axis) and power dissipated at 1 kHz by the MCn transistor, $P^{MCn}_{1\,kHz}$ (left axis).

amplitude (−15 dBm) and frequencies f_1 and $f_2 = f_1 +$ 1 kHz to its input. By sweeping f_1 from 2 to 3 GHz (and always keeping 1 kHz between the two tones) we simulated (harmonic balance simulation, using the ADS CAD software) the voltage gain A_v inside this frequency range and the amplitude of the power dissipated by the MCn transistor at 1 kHz, $P^{MCn}_{1\,kHz}$.

In Fig. 9 we show $P^{MCn}_{1\,kHz}$ and A_v squared (note that according to (5) the power dissipated at f_2–f_1 by an active device depends on the squared voltage gain). The two curves shown in the figure agree well in the band of interest. From the $P^{MCn}_{1\,kHz}$ curve (solid line, left axis), it is possible to estimate that the LNA −3 dB bandwidth is BW = 402 MHz and that its central working frequency is $f_0 = 2.398$ GHz. If we directly use the $A_v \times A_v$ curve (dashed line, right axis), the values obtained are BW = 414 MHz and $f_0 = 2.400$ GHz. The error between the original BW and f_0 characteristics and the values obtained from the low-frequency dissipated power is 3% and 0.1%, respectively. This demonstrates that some electrical characteristics of the LNA at 2.4 GHz can be effectively estimated by monitoring the power dissipated by one of its devices at 1 kHz (which, as has been shown in the previous section, can be derived by thermal measurements).

In the previous simulations, nominal condition parameters were considered. In order to analyze how process variations and mismatching can affect the technique, we performed a MonteCarlo simulation of the LNA (by using PSS plus PAC analysis of Cadence CAD software),

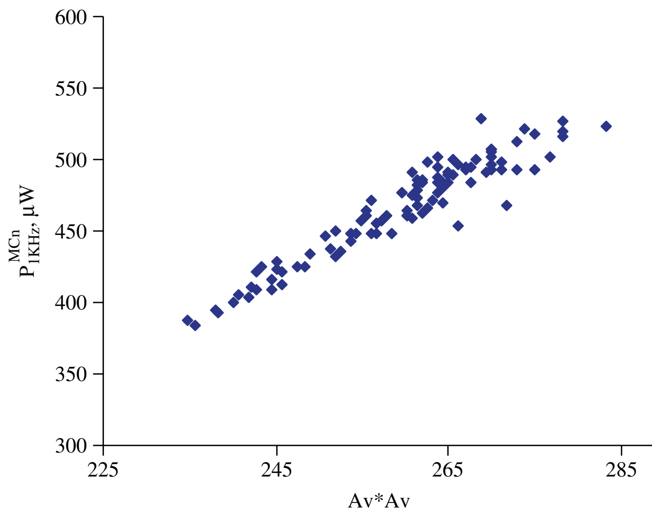

Fig. 10. Correlation between the LNA squared voltage gain at 2.4 GHz and the power dissipated by the MCn transistor at 1 kHz from MonteCarlo simulations.

considering both chip-to-chip process variations and intra-chip random mismatching. In this simulation, two tones of −15 dBm with fixed frequencies of 2.4 GHz and 2.400001 GHz were applied to the input.

Results are shown in Fig. 10, where the power dissipated by the MCn transistor at 1 kHz is plotted for the different simulations against the squared value of the LNA voltage gain at 2.4 GHz. According to the figure, the two magnitudes are strongly correlated, which demonstrates the robustness of the technique with regard to process variations.

5. Conclusions

In this paper we have presented a novel strategy for observing electrical characteristics of analogue/RF circuits. It is based on measuring the amplitude of some spectral components of the temperature sensed at the silicon surface, close to the circuit under test.

This testing and characterization strategy has the following advantages:

(i) The circuit under test is not electrically loaded. Therefore, its electrical performances are unaffected.
(ii) There is no need to have direct access to electrical nodes of the CUT to measure the electrical signals.
(iii) Temperature sensors can be embedded within the CUT, allowing in-field testing and characterization.
(iv) The information is read at f_2–f_1, independently of the absolute values of f_1 and f_2. Thus, temperature sensors and filters in the testing/characterizing system are designed for this low frequency, independently of the specific spectral band at which f_1 and f_2 are placed.

The experimental results show that it is possible to measure power amplitudes below 1 μW using differential temperature sensors embedded within the CUT. Simulated results illustrate an application of the technique: the estimation of the bandwidth and central frequency of a 2.4 GHz LNA designed using a 0.35 μm CMOS technology.

Acknowledgements

This work was partially supported by Projects TEC2005-06787-C02-01MIC and TEC2005-02739MIC of the Spanish MEC and FEDER funds. The authors would like to thank Dr. Joaquim Puigdollers for his support in the experimental set-up. Eduardo Aldrete is grateful for the support of the DURSI of the Autonomous Government of Catalonia.

References

[1] S.S. Akbay, A. Chatterjee, Feature extraction based built-in alternate test of RF components using a noise reference, in: Proceedings of the 22nd VLSI Test Symposium, April 2004, pp. 273–278.
[2] K.B. Schaub, J. Kelly, Production Testing of RF and System-on-a-Chip Devices for Wireless Communications, Artech House, Boston, 2004.
[3] J. Liobe, M. Margala, Fault diagnosis of a GHz CMOS LNA using high-speed ADC-based BIST, in: Proceedings of the IEEE International Workshop on Current and Defect Based Testing, April 2004, pp. 85–89.
[4] J. Dabrowski, BiST model for IC RF-transceiver front-end, in: Proceedings of the 18th IEEE International Symposium on Defect and Fault Tolerance in VLSI Systems, November 2003, pp. 672–679.
[5] J.Y. Ryu, B.C. Kim, A new design for built-in self-test of 5 GHz low noise amplifiers, in: Proceedings of the IEEE International SOC Conference, September 2004, pp. 324–327.
[6] A. Soldo, A. Gopalan, P.R. Mukund, M. Margala, A current sensor for on-chip, non-intrusive testing of RF systems, in: Proceedings of the 17th International Conference on VLSI Design, 2004, pp. 1023–1026.
[7] A. Gopalan, T. Das, C. Washburn, P.R. Mukund, An ultra-fast, on-chip BiST for RF low noise amplifiers, 18th International Conference on VLSI Design, January 2005, pp. 485–490.
[8] M.G. Mendez-Rivera, A. Valdes-Garcia, J. Silva-Martinez, E. Sanchez-Sinencio, An on-chip spectrum analyzer for analog built-in testing, Journal of Electronic Testing: Theory and Applications 21 (2005) 205–219.
[9] J. Altet, S. Dilhaire, S. Volz, J.M. Rampnoux, A. Rubio, S. Grauby, L.D. Patino, W. Claeys, J.B. Saulnier, Four different approaches for the measurement of IC surface temperature: application to thermal testing, Microelectron. J. 33 (2002) 689–696.
[10] N. Nenadovic, S. Mijalkovic, L.K. Nanver, L.K.J. Vandamme, V. d'Alessandro, H. Schellevis, J.W. Slotboom, Extraction and modeling of self-heating and mutual thermal coupling impedance of bipolar transistors, IEEE J. Solid-State Circuits 39 (10) (2004) 1764–1772.
[11] Agilent E4438C ESG Vector Signal Generator, Data Sheet, Set, 2002, p. 23.
[12] J. Altet, A. Rubio, E. Schaub, S. Dilhaire, W. Claeys, Thermal coupling in integrated circuits: application to thermal testing, IEEE J. Solid-State Circuits 36 (1) (2001) 81–91.
[13] S. Dilhaire, E. Schaub, W. Claeys, J. Altet, A. Rubio, Localisation of heat sources in electronic circuits by microthermal laser probing, Int. J. Therm. Sci. 39 (2000) 544–549.
[14] B. Razavi, Design of Analog CMOS Integrated Circuits, McGraw-Hill International Edition, 2001.